JOURNAL OF SOLID STATE CHEMISTRY 33, 1–11 (1980)

About SnF_2 Stannous Fluoride. II. Crystal Structure of β- and γ-SnF_2

G. DENES, J. PANNETIER, AND J. LUCAS

Université de Rennes-Beaulieu, Laboratoire de Chimie Minérale D, Laboratoire Associé au CNRS No. 254, Avenue du Général Leclerc, 35042 Rennes Cedex, France

Received March 6, 1978; in revised form March 20, 1979

Two new structural modifications (β and γ) of SnF_2 have been prepared and their structures refined from X-ray powder data by analogy with high- and low-pressure TeO_2. Both structures are described and discussed using Galy's and Brown's models. Topological relationships to rutile and cristobalite structures are outlined.

Introduction

The crystal chemistry and phase transitions of the MF_2 fluorides have been investigated by several authors. These compounds crystallize in the fluorite-type structure for the largest cations and in the rutile type for the 3*d* transition metals; BeF_2 and α-PbF_2 present respectively the SiO_2- and $PbCl_2$-type structures. However, very few studies have been devoted to either SnF_2 or GeF_2, although their position in the middle of the IVB column gives them intermediate properties between covalent (C, Si) and ionic (Pb) fluorides; moreover, the presence of a lone pair on the divalent cation leads to strong distortions of the coordination polyhedra.

Recent investigations of the crystal structure (*1*) and crystal chemistry (*2*) of monoclinic α-SnF_2 show the following features: a rather molecular behavior (Sn_4F_8 tetramers), a strong stereoactivity of the lone pairs, and a topological relationship to rutile. We report in this paper the crystal structure determination of two new crystalline phases β- and γ-SnF_2 and their topological relationships to rutile and cristobalite structures.

Experimental

1. Sample Preparation

γ-SnF_2 is obtained by heating α-SnF_2 above 180°C (*3*) under vacuum or inert atmosphere; upon cooling it transforms to β-SnF_2 below 67°C (second-order displacement transition). Both β- and γ-SnF_2 are metastable below $\simeq$110°C and a small pressure is sufficient to induce the transformation to α-SnF_2. The $\alpha \rightarrow \gamma$ transition is first order, reconstructive, and single crystals of α-SnF_2 disintegrate on passing through this transition: no single crystals of β- or γ-SnF_2 could be obtained. The room-temperature density of β-SnF_2 determined by CCl_4 displacement is 4.82 g/cm^3.

2. Unit-cell Parameters

The unit-cell parameters were obtained from X-ray powder data (at room temperature for β-SnF_2 and at 80°C for γ-SnF_2) by using a trial and error method developed by Louër and Louër (*4*). The 21 reflections of each powder pattern were used; the cubic, tetragonal, hexagonal, and orthorhombic

0022-4596/80/070001-11$02.00/0

systems were tested with the restrictions

— $a, b, c \leq 25$ Å,
— ESD $(\theta) = 0.22°$,
— ESD (density) $= 0.10$ g/cm^3;

for both phases, a single solution was obtained, respectively orthorhombic and tetragonal for β- and γ-SnF_2 with $Z = 4$. The monoclinic system was also tested (*5*) with the restrictions

— $a, b, c < 15$ Å,
— $\beta < 110°$,
— $V < 250$ Å^3,

but no solution was obtained. The refined cell parameters are given in Table I. De Wolff's criterion (*6*) for the reliability of powder pattern indexing gives figures of merit $M_{20} = 27$ for β-SnF_2 and $M_{20} = 30$ for γ-SnF_2, which are good guarantees for correct indexing.

3. *Intensity Measurements*

Data were collected as previously described (*7*). The sample of β-SnF_2 was prepared by heating a carefully ground sample of α-SnF_2 at 190°C for 1 h and then quenching; the sample of β-SnF_2 thus obtained was not reground in order to avoid a $\beta \rightarrow \alpha$ reconversion (*3*). The γ-SnF_2 sample was prepared *in situ* in a high-temperature furnace adapted for X-ray diffraction (*8*) by heating to 190°C and then cooling down to 80°C; the experiment was run under dry nitrogen. Because of the high X-ray absorption of the aluminium windows of the high-temperature device, the accuracy of the data is somewhat lower for γ-SnF_2 than for β-SnF_2.

4. *Structure Refinements*

Both structures were determined by analogy to the structures of GeF_2 (*9*) and high-pressure (HP) TeO_2 (*10*) for β-SnF_2 and with the paratellurite TeO_2 (*10*) for γ-SnF_2. This isotypism was suggested by the following points:

— the similar cell parameters (Table I);
— the same valence shell electronic configurations of Sn^{2+}, Ge^{2+}, and Te^{4+}, with an unshared electronic pair known to be stereoactive;
— the pseudo-body-centred tetragonal arrangement of the cations in GeF_2 and TeO_2 as in α-SnF_2 (hence, the difference between α-, β-, and γ-SnF_2 must be due only to the anions distribution);
— the observed X-ray reflections agree with the space groups given for TeO_2 and GeF_2 ($P2_12_12_1$ (No. 19) for β-SnF_2 and $P4_12_12$ (No. 92) (or enantiomorphic $P4_32_12$) for γ-SnF_2; moreover, all the (hkl) reflections with l odd are very weak as they are in GeF_2 and TeO_2, which comes from the

TABLE I

UNIT-CELL PARAMETERS

	HP-TeO_2[a]	GeF_2	β-SnF_2	γ-SnF_2[b]	LP-TeO_2
a(Å)	4.6053 (6)	4.682 (1)	4.9889 (7)	5.0733 (9)	4.8052 (3)
b(Å)	4.8557 (6)	5.178 (1)	5.1392 (6)	a	a
c(Å)	7.5300 (10)	8.312 (1)	8.4777 (14)	8.4910 (33)	7.6021 (8)
V(Å^3)	168.39 (7)	201.51 (11)	217.36 (9)	218.54 (16)	175.53 (4)
ρ_{obs} (g/cm^3)		3.7	4.82		
ρ_{calc} (g/cm^3)	6.30	3.64	4.79	4.76	6.04
Reference	(*10*)	(*9*)	This work	This work	(*10*)

[a] At 19.8 kbar.
[b] at 80°C.

TABLE II

FINAL ATOMIC COORDINATES

	β-SnF_2	GeF_2 (*9*)	HP-TeO_2(*10*)	γ-SnF_2 (80°C)	LP-TeO_2 (*10*)
x	0.274 (5)	0.266 (4)	0.274 (2)	0.011 (30)	0.025 (1)
y	0.023 (7)	0.008 (5)	0.012 (3)	0.011 (30)	0.025 (1)
z	0.130 (5)	0.131 (3)	0.117 (2)	0.0	0
B	0.5[a]	[b]	0	2.9 (1.1)	0
x	0.541 (6)	0.528 (24)	0.549 (2)	0.102 (22)	0.139 (1)
y	0.163 (5)	0.082 (24)	0.120 (2)	0.305 (18)	0.262 (1)
z	0.996 (3)	0.982 (18)	0.940 (1)	0.171 (13)	0.187 (1)
B	0.8[a]	[b]	1.08 (16)	0 (3.9)	0.63 (15)
x	0.378 (4)	0.433 (18)	0.406 (2)		
y	0.202 (2)	0.246 (29)	0.234 (2)		
z	0.385 (4)	0.279 (18)	0.333 (1)		
B	0.8[a]	[b]	1.08 (16)		
Space group	$P2_12_12_1$	$P2_12_12_1$	$P2_12_12_1$	$P4_12_12$ ($P4_32_12$)	$P4_12_12$ ($P4_32_12$)

[a] Not refined.

[b] Anisotropic thermal parameters used.

existence of a cationic tetragonal sublattice with parameter $c' = c/2$);

— the β-SnF_2 space group is a subgroup of order 2 of the γ-SnF_2 space group in agreement with the second-order nature of the $\beta \rightleftarrows \gamma$ reversible transition (*3*);

— a second harmonic generation test on β-SnF_2 gives a weak signal which indicates a noncentrosymmetrical space group.

The structure refinements were carried out with the following conditions:

— For β-SnF_2: 51 (*hkl*) reflections/21 measured intensities; three kinds of atoms Sn, F(1), F(2) in the general position (4*a*); final discrepancy factors $R = 7.5\%$ and $R_w = 10.8\%$.

— For γ-SnF_2: 27 (*hkl*) reflections/15 measured intensities; two kinds of atoms Sn in (*xx*0) and F in (*xyz*); final discrepancy factors $R = 8.4\%$ and $R_w = 12.5\%$.

In both cases, we used the Cromer–Waber scattering factors (*11*) and the atoms were first positioned as in GeF_2 and TeO_2. The least-squares refinement was performed with a local program (*12*).

The final atomic coordinates given in Table II are not very different from those of GeF_2 and TeO_2. It is worth noting that there are eight possible positions for the origin of the unit cell in $P2_12_12_1$ and the crystal structures of GeF_2 (*9*) and HP–TeO_2 (*10*) were solved with different origins; all the results given in this paper refer to the high-pressure TeO_2 cell[1].

Description of the Structures

1. *Stereochemistry of* Sn^{2+}

As for α-SnF_2 (*2*), a good description of the environment of Sn^{2+} is obtained by the following two models.

(*a*) *the Galy–Andersson lone-pair model* (*13*) *which is based on the electrostatic repulsion theory of Gillespie and Nyholm* (*14*). The activity of the lone pair *E* can be shown by comparing the molecular volume per anion

[1] $(x, y, z)_{GeF_2} = (1/2 - x, y, z)_{TeO_2}$.

between different Sn^{2+}- and Sn^{4+}-containing structures. For this, two volumes must be defined:

$$V_1 = \frac{\text{molecular volume}}{\text{number of anions in the molecule}},$$

$$V_2 = \frac{\text{molecular volume}}{\text{number of anions}} + \text{lone pairs in the molecule}.$$

According to our previous study (*2*), V_1 ranges from 16 to 40 Å^3 while V_2 is almost constant and equal to 16–20 Å^3. For the present structures, one obtained V_1 = 27.2 Å^3 (β) and 27.3 Å (γ) while V_2 = 18.1 Å^3 (β) and 18.2 Å^3 (γ), clearly demonstrating that the tin lone pair (E) is still active in β- and γ-SnF_2 and requires a volume comparable to that of a fluoride anion.

The interatomic distances are given in Table III; in β-SnF_2, tin atoms have an octahedral coordination SnF_5E (one short axial bond and four intermediate equatorial bonds), but, in γ-SnF_2, one observes a triangular bipyramid SnF_4E (two short equatorial and two intermediate axial Sn–F bonds). The unusual SnF_5E octahedron (Fig. 1) was first observed in α-SnF_2 (*1, 2*) and corresponds to an sp^3d^2 hybridization; the SnF_4E triangular bipyramid (Fig. 2) is more common in stannous compounds (see Sn_2OF_2 (*15*) for instance) and is also observed in paratellurite but with shorter bond lengths.

The geometrical characteristics of the SnF_5E octahedron and SnF_4E bipyramid have been calculated according to Galy's model by using a local program (*3*) and are given in Tables IV and V. Although β-SnF_2, GeF_2, and HP-TeO_2 are isostructural, the coordination polyhedra around the cation are rather different:

— in β-SnF_2: SnF_5E octahedron (E + F + 4F);

TABLE III

INTERATOMIC DISTANCES[a]

β-SnF_2		γ-SnF_2	
Sn_1–F_{11}	1.89 (3)	Sn_1–F_1	2.13 (15)
Sn_1–F_{14}	2.26 (3)	Sn_1–F_2	2.13 (15)
Sn_1–F_{22}	2.40 (2)	Sn_1–F_6	2.32 (18)
Sn_1–F_{21}	2.41 (4)	Sn_1–F_7	2.32 (18)
Sn_1–F_{23}	2.49 (3)	Sn_1–F_3	3.27 (13)
Other		Sn_1–F_4	3.27 (13)
distances >	3.50 Å	Sn_1–F'_6	3.35 (18)
F_{11}–Sn_1	1.89 (3)	Sn_1–F'_7	3.35 (18)
F_{11}–Sn_4	2.26 (3)	Other	
F_{21}–Sn_2	2.40 (2)	distances	>3.89 Å
F_{21}–Sn_1	2.41 (4)	F_1–Sn_1	2.13 (15)
F_{21}–Sn_3	2.49 (3)	F_1–Sn_5	2.32 (18)
		F_1–Sn_3	3.27 (13)
		F_1–Sn'_5	3.35 (18)

[a] The number of each atom is defined as follows:

(a) In β-SnF_2:

Sn_j (j = 1, 4) for the cations;

F_{ij} (i = 1, 2; j = 1, 4) for the anions.

j is the number of each equivalent position ($P2_12_12_1$):

$j = 1(x, y, z)$,

$j = 2(1/2 - x, \bar{y}, 1/2 + z)$,

$j = 3(1/2 + x, 1/2 - y, \bar{z})$,

$j = 4(\bar{x}, 1/2 + y, 1/2 + y, 1/2 - z)$.

(b) In $\gamma - SnF_2$: Sn_i and F_i, i being the number of each equivalent position ($P4_12_12$):

$i = 1(x, y, z)$,

$i = 3(\bar{x}, \bar{y}, 1/2 + z)$

$i = 5(1/2 - y, 1/2 + x, 1/4 + z)$,

$i = 7(1/2 + y, 1/2 - x, 3/4 + z)$,

$y = 2(y, x, \bar{z})$,

$y = 4(y, x, 1/2 - z)$

$y = 6(1/2 - x, 1/2 + y, 1/4 - z)$,

$y = 8(1/2 + x, 1/2 - y, 3/4 - z)$.

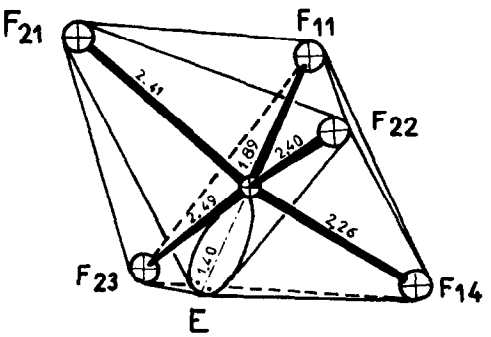

FIG. 1. SnF_5E octahedron in β-SnF_2.

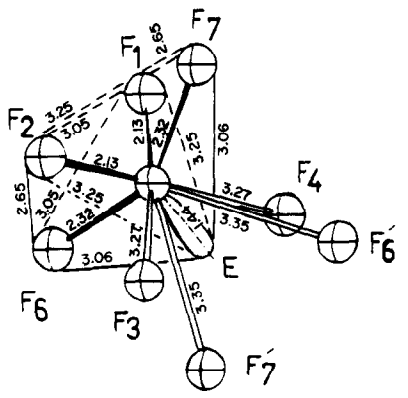

FIG. 2. SnF_4E triangular bipyramid in γ-SnF_2.

TABLE IV

GEOMETRICAL CHARACTERISTICS OF THE SnF_5E OCTAHEDRON IN α- AND β-SnF_2 AND TeO_5E OCTAHEDRON IN TeO_2 AT 19.8 kbar

Value[a]	α-SnF_2	β-SnF_2	HP-TeO_2 (*10*)
a_1(Å)	3.25	3.38	3.11
a_2(Å)	2.80	2.91	2.81
d_1(Å)	2.34	2.39	2.19
d_2(Å)	2.05	1.89	1.91
d_{M-E}(Å)	1.17	1.40	1.58
ψ(°)	79.1	85	86.5

[a] All these geometrical values are defined in Ref. (*13*) (octahedral model).

— in HP-TeO_2: TeO_5E polyhedron intermediate between octahedron and trigonal bipyramid ($E+4O+O$);

— in GeF_2: GeF4E polyhedron intermediate between trigonal bipyramid and tetrahedron ($E+3F+F$).

(*b*) *Brown's valence model* (*19*). Tin atoms in β-SnF_2 have the unusual $\mathscr{D}$ configuration (one strong and four intermediate bonds) previously observed in α-SnF_2; in γ-SnF_2, the more common $\mathscr{B}$ configuration is observed. In both cases, and in agreement with Brown's model, the polyhedron distortion is such that weak bonds occur opposite strong bonds and bonds of intermediate strength opposite each other.

However, if all Sn–F distances less than 3.4 Å in γ-SnF_2 are taken into account, the SnF_4E bipyramid does not result from the distortion of an octahedron (as assumed in Brown's model) but from a square antiprism (Fig. 3). Gillespie has shown in his book (*20*) that, among the six possible MX_8 polyhedra, it is the square antiprism which leads to the

TABLE V

GEOMETRICAL CHARACTERISTICS OF THE TRIANGULAR BIPYRAMID IN γ-SnF_2, TeO_2 AND SOME OTHER STANNOUS FLOURIDE COMPOUNDS

Value[a]	γ-SnF_2	TeO_2 (*10*)	Sn_2OF_2 (Sn(2)) (*15*)	$KsnF_3, \frac{1}{2}H_2O$ (*16*)	$NaSn_2F_5$ (*17*)	$Na_4Sn_3F_{10}$ (*18*) Sn(1)	$Na_4Sn_3F_{10}$ (*18*) Sn(2)
a_1(Å)	3.25	2.904	2.632	2.80	2.91	2.83	2.78
a_2(Å)	3.45	2.703	3.079	2.81	2.77	2.75	2.83
$k=a_1/a_2$	0.95	1.07	0.85	0.99	1.05	1.03	0.98
d_1(Å)	2.13	1.919	2.106 (Sn–O)	2.02	2.07	2.04	2.04
d_2(Å)	2.37	2.087	2.388 (Sn–F)	2.27	2.37	2.32	2.26
l(Å)	4.46	4.134	4.759	4.43	4.50	4.43	4.44
d_{M-E}(Å)	1.44	1.26	0.635	0.96	1.09	1.00	0.91
α(°)	140	163.9	170.5	155.1	142	146.3	158.3
β(°)	99	98.3	77.3	87.5	89	87.8	85.7
θ(°)	74	53.1	70.7	57.8	40	45.3	59
ψ(°)	74	53.1	70.7	57.8	62	61.4	59

[a] All these geometrical values are defined in Ref. (*13*) (bipyramidal model). l = axial anion–anion distance.

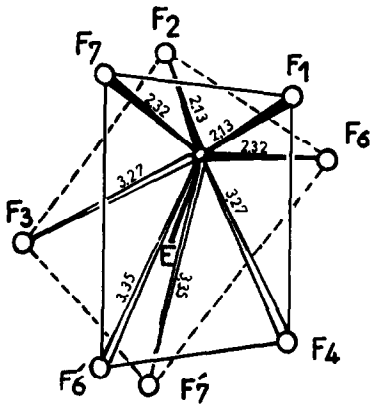

FIG. 3. Square antiprism distorted by the lone pair in γ-SnF_2.

weakest X–X electrostatic repulsions; the possible distortions of both the cube and the square antiprism by a lone-pair were described by Orgel (*21*) (Fig. 4), but only distortions about a fourfold axis were known, for insance, in SnO or PbO (*22*) for the cube (Fig. 4b) and in $PbCu(OH)_4Cl_2$ (*23*) for the square antiprism (Fig. 4d). The polyhedron observed in γ-SnF_2 (Figs. 3 and 4e) is an example of a distortion which does not keep the fourfold axis; closely related polyhedra are observed in SnFCl (*24*) and α-PbF_2. Therefore, the size of Sn^{2+} cation is such that it can accommodate a coordination deriving either from an octahedron (as outlined by Brown) or from a cube; the latter conclusion is supported by the existence of $MSnF_4$ compounds (M = Pb, Ba, Sr) whose structures are related to the fluorite type (*25*).

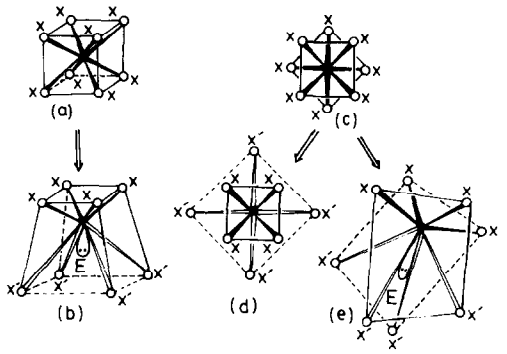

FIG. 4. Structures obtained by distorting a cube, (a) → (b), and a square antiprism, (c) → (d), about a fourfold axis, described by Orgel (*21*); distortion occurring in γ-SnF_2, (c) → (e).

2. *Fluorine Stereochemistry*

In β-SnF_2, GeF_2 and HP-TeO_2, there are two kinds of anions: one is a bridging anion (shared by two cations) while the coordination of the second kind depends on the size of the cation. It is in a threefold coordination in β-SnF_2 (Fig. 5), in a bridging position in HP-TeO_2, but, in GeF_2, this second anion is almost terminal (bonded to only one cation).

In the tetragonal structure (γ-SnF_2) all anions are in a bridging position.

3. *Topological relationships*

(*a*) *Cationic lattice.* In the three structures α-, β- and γ-SnF_2, tin atoms have a pseudo-body-centred arrangement which also exists in TeO_2 and GeF_2; cation displacements from ideal positions are small:

— in β-SnF_2	0.024 **a**/0.023 **b**/0.005 **c**
— in HP-TeO_2	0.016 **a**/0.008 **b**/0.006 **c**
— in GeF_2	0.024 **a**/0.005 **b**/0.008 **c**
— in γ-SnF_2	0.01 **a**/0.01 **b**/ no displacement along **c**
— in LP-TeO_2	0.03 **a**/0.03 **b**/ no displacement along **c**

This distortion is visualized in Fig. 6 which compares β- and γ-SnF_2 to rutile.

(*b*) *Polyhedra linkage.* The SnF_5E octahedra in β-SnF_2 share one vertex which leads

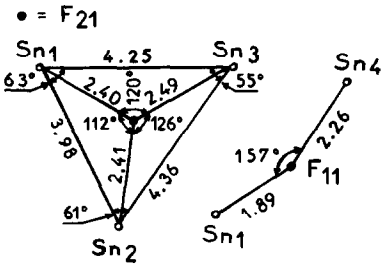

FIG. 5. Coordination of the two kinds of fluorine in β-SnF_2.

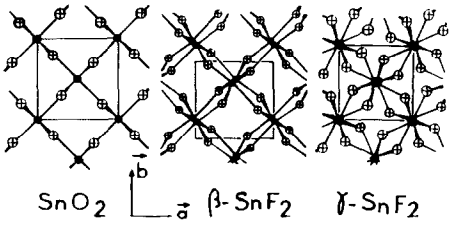

FIG. 6. Distortion of the pseudo-body-centered arrangement of tin atoms in β- and γ-SnF_2.

to a three-dimensional framework: each F(1) is shared between two octahedra while F(2) is common to three octahedra as in the rutile structure. This gives rise to rows of octahedra running along the c axis (Fig. 7); this projection of the SnO_2 and β-SnF_2 structures in the plane defined by the directions [110] and [001] clearly shows the role of lone pairs in the distortion of the structure and the reason for doubling the c axis.

These rows of octahedra running along the c axis no longer exist in γ-SnF_2. Instead the SnF_4E bipyramids are linked to each other in such a way that they form Sn_6F_6 rings similar to the Si_6O_6 rings observed in the cristobalite structure; each cation is common to six rings and each anion to four rings. This comparison between high-temperature β-cristobalite (space group $I\bar{4}2d$ (*26*)), low-temperature α-cristobalite (space group $P4_12_12$ (*27*)), and γ-SnF_2 (space group $P4_12_12$) is presented in Figs. 8 and 9: the transition from β- to α-cristobalite can be visualized as a lengthening of the AD diagonal (Fig. 8) and a shortening of CF; the same distortion occurs in γ-SnF_2 but to a greater extent.

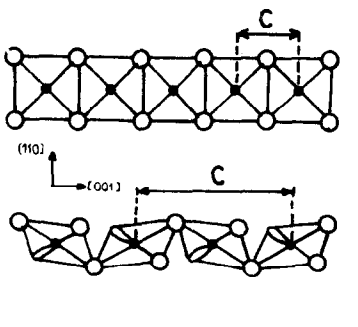

FIG. 7. Rows of octahedra along c in β-SnF_2 and SnO_2 (rutile type).

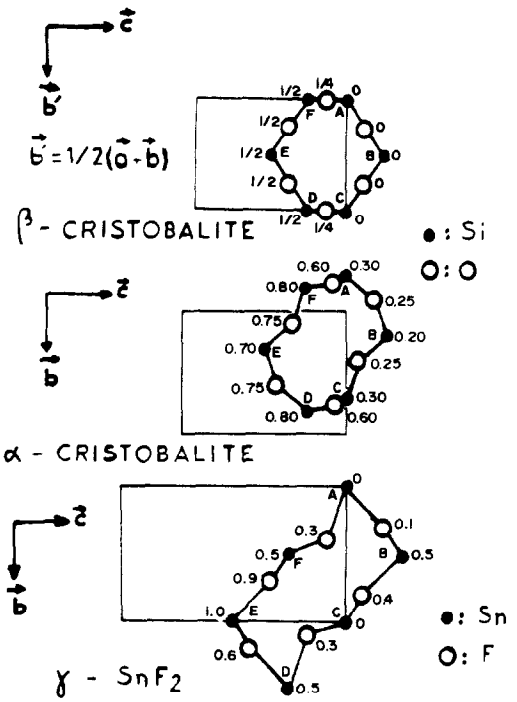

FIG. 8. Si_6O_6 rings in β- and α-cristobalite and Sn_6F_6 rings in γ-SnF_2. The z coordinate of each atom is indicated. The length of each diagonal is

— in β-cristobalite: AD = BE = CF = 5.91 Å;

— in α-cristobalite: AD = 6.25 Å, BE = 5.78 Å, CF = 5.40 Å;

— in γ-SnF_2: AD = 8.20 Å, BE = 7.12 Å, CF = 4.10 Å.

(*c*) *Anionic lattice.* The rutile structure can be described from the hexagonal close packing of the anions (*28*) and the same description also holds for β-SnF_2 and HP-TeO_2 with the difference being that the close-packed layers contain both anions and lone pairs (the same fluorine lone-pairs packing is observed in α-SnF_2 (*2*)). This hexagonal close packing of anions disappears in γ-SnF_2 which exhibits as paratellurite the same packing of anions as α- and β-cristobalite: an open anionic network with vacancies at the center of the rings. A strong

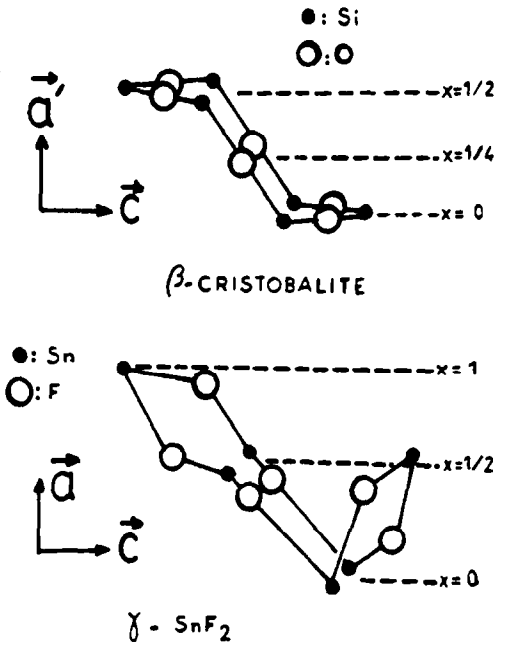

FIG. 9. Conformation of Si_6O_6 and Sn_6F_6 rings in β-cristobalite and γ-SnF_2.

increase in compactness (≈46%) occurs at the cristobalite → stishovite (high-pressure phase of SiO_2, of rutile structure (*29–32*)) transition, resulting from the transformation of an open to a compact oxygen atom lattice. No increase of density is observed in the $\gamma \rightarrow \beta$ transition of SnF_2 or paratellurite → HP-TeO_2. However, a similar environment of anions is observed in both structures:

— in cristobalite, γ-SnF_2, each anion (O or F) is surrounded by 6 anions (5 in paratellurite)

—in the rutile type; each anion is surrounded by 12 anions, but if one considers the lone pairs E as anions, in γ-SnF_2 and paratellurite, each anion (O, F, or E) is surrounded by 10 or 14 anions; then their structures are as compact as that of β-SnF_2 and HP-TeO_2, but with a different packing of anions; this explains why no increase in compactness occurs at the transitions $\gamma \rightarrow$ β-SnF_2 and paratellurite → HP-TeO_2.

Furthermore, the presence of lone pairs inside the rings in γ-SnF_2 and TeO_2 which do not exist in the analogous cristobalite type prevents formation of insertion compounds ABX_2 ($KFeO_2$ type) by double substitution as observed in cristobalite ($Si^{4+}/K^{+}Fe^{3+}$).

(*d*) *Cristobalite–rutile GeF_2 Transformations.* Both the tetrahedral and the octahedral coordinations of Si^{4+} and Ge^{4+} are well known. A mechanism of transformation of SiO_2 from cristobalite to rutile structures involving rotation of tetrahedra was recently proposed (*33, 34*). The crystal structures of SnF_2 and TeO_2 can be treated as intermediate stages of this transformation, which can be divided into two parts: first a cationic rearrangement, the polyhedra remaining tetrahedra; then, movements of anions involving the transformation of tetrahedra into octahedra.

These transformations are explained in Fig. 10 and 11. The translation of cations is shown in Fig. 10 and 6; this motion takes place in the (**a**, **b**) plane; the vectors of translation of the four cations of the unit cell are the following: $\mathbf{T}_1'$ and $\mathbf{T}_1 = (0, 0, 0)$, $\mathbf{T}_2'$ and $\mathbf{T}_2 = (x, 0, 0)$, $\mathbf{T}_3'$ and $\mathbf{T}_3 = (0, x, 0)$, $\mathbf{T}_4'$ and $\mathbf{T}_4 = (x, x, 0)$, with $x = -0.10$ from β to α-cristobalite, and -0.40 from α-cristobalite to γ-SnF_2.

This first part of the cristobalite → rutile transformation involves a translation of the tetrahedra which are progressively distorted (SnF_4E and TeO_4E bipyramids can be

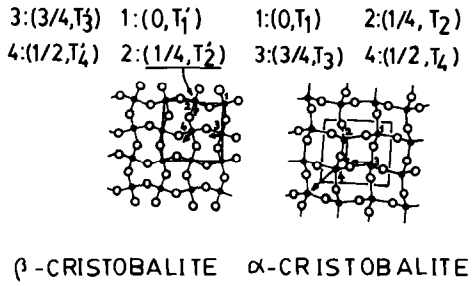

FIG. 10. Movement of the cations in the (**a**, **b**) plane from β-cristobalite to γ-SnF_2.

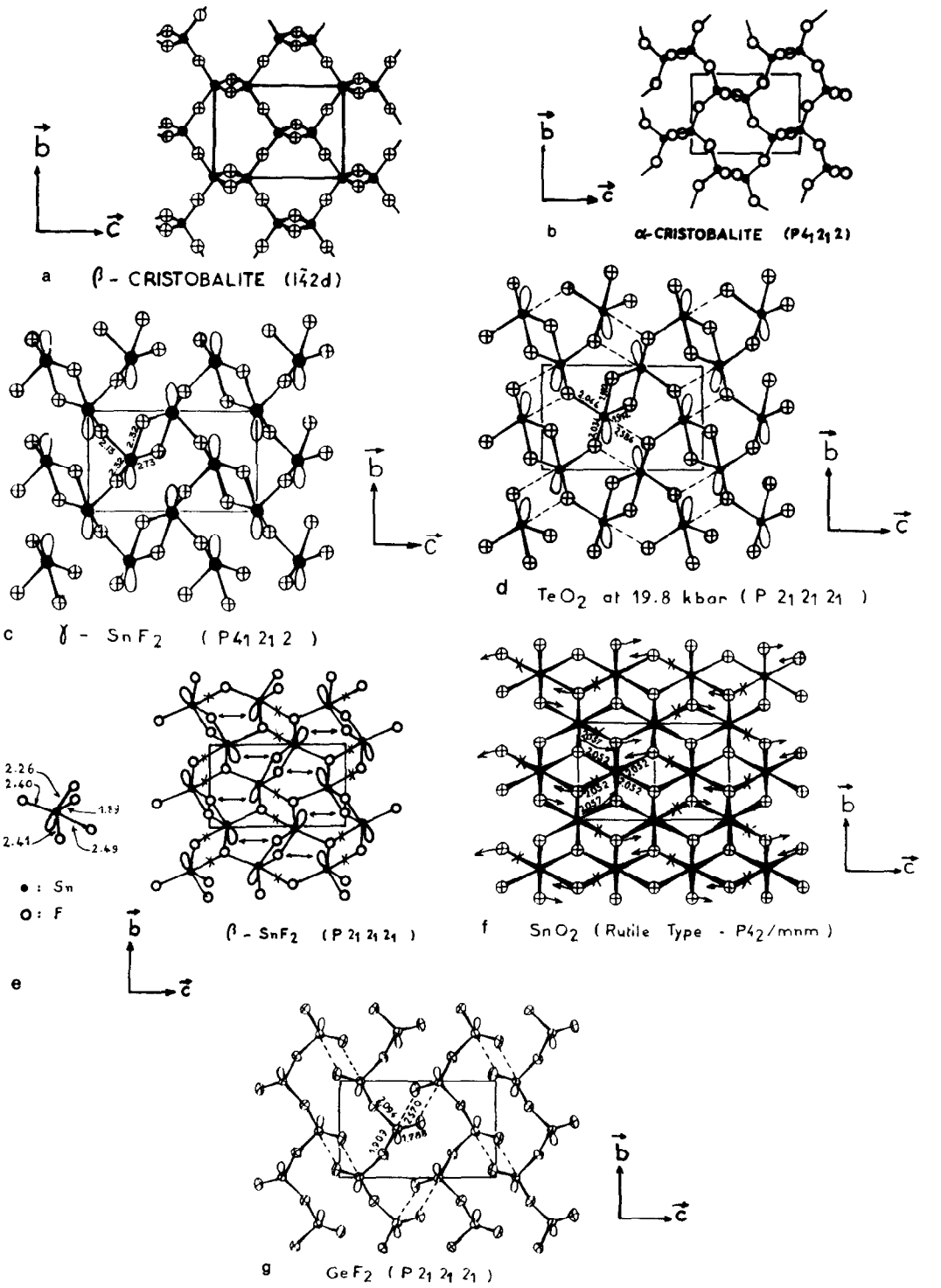

FIG. 11. Cristobalite → rutile and rutile → GeF_2 transformations (a) β-cristobalite, (b) α-cristobalite, (c) γ-SnF_2 (d) TeO_2 at 19.8 kbar, (e) β-SnF_2, (f) SnO_2, (g) GeF_2.

considered as tetrahedra strongly distorted by the lone pair E) and a distortion of Si_6O_6 and Sn_6F_6 rings (Figs. 11a–c).

In the second part of the transformation, only motions of anions occur, the cationic lattice remaining a pseudo-body centered one as in γ-SnF_2, while the tetrahedra are progressively transformed to octahedra (Fig. 11c–f). The following stages are observed.

— γ-SnF_2 and paratellurite (Fig. 11c): bipyramid SnF_4E and TeO_4E; bridging anions.

— TeO_2 at 19.8 kbar (Fig. 11d): intermediate between TeO_4E bipyramid and TeO_5E octahedron; one oxygen is still bridging, the other one is in 2 + 1 coordination; Te_6O_6 rings begin to be divided into two parts.

— β-SnF_2 (Fig. 11e): is SnF_5E octahedron; one fluorine is still bridging, the other one is being shared between three Sn atoms; the rings have disappeared; there are rows of octahedra as in rutile but they share only a vertex:

— SnO_2 (Fig. 11f): SnO_6 octahedra; all the oxygen atoms are in a threefold coordination site.

The rutile → GeF_2 transformation involves only a motion of anions which depends on the size of the cation. From SnO_2 to β-SnF_2, the bonds indicated by crosses (Fig. 11f) disappear and result in a displacement of anions as indicated by the arrows. From β-SnF_2 to high-pressure TeO_2, and from high-pressure TeO_2 to GeF_2, the bonds indicated by crosses disappear (Figs. 11e and 11d) and result in the chain polymer structure of GeF_2 (Fig. 11g). In this structure, the GeF_3E tetrahedra are linked by sharing bridging fluorines. The stability of this structure in the solid state is due to van der Waals bonds between neighboring chains, in agreement with the low melting point (110°C) (*35*).

Acknowledgment

We are very grateful to D. Louër, Laboratoire de Cristallochimie, Rennes, for supplying us with his automatic indexing programs and for stimulating discussions.

References

1. R. C. McDonald, H. Ho-Kuen Hau, and K. Eriks, *Inorg. Chem.* **15**, 4 (1976).
2. G. Denes, J. Pannetier, J. Lucas, and Le Marouille, *J. Solid State Chem.* **30**, 335 (1979).
3. G. Denes, Thèse d'Etat, Rennes (1978).
4. D. Louër and M. Louër, *J. Appl. Cryst. allogr.* **5**, 271 (1972).
5. D. Louër and Pivol, A Fortran IV Program for Automatic Indexing of Powder Patterns in Monoclinic System," unpublished.
6. P. M. De Wolff, *J. Appl. Crystallogr.* **1**, 108 (1968).
7. G. Fonteneau, H. L'Helgoualch, and J. Lucas, *Mater. Res. Bull.* **12**, 25 (1977).
8. P. Barret, N. Gerard, and G. Watelle-Marion, *Bull. Soc. Chim. Fr.* **8**, 3172 (1968).
9. J. Trotter, M. Akhtar, and N. Bartlett, *J. Chem. Soc. Abstr.* **30**.
10. T. G. Worlton and R. A. Beyerlein, *Phys. Rev. B* **12**, 1899 (1975).
11. D. T. Cromer and J. T. Waber, *Acta Crystallogr.* **18**, 114 (1965).
12. H. L'Helgoualch, G. Fontenau and J. Pannetier, 'Maryse' A Structure Refinement Program for Powder Data," unpublished.
13. J. Galy, G. Meunier, S. Andersson, and A. Aström, *J. Solid State Chem.* **13**, 142 (1975).
14. R. J. Gillespie and R. S. Nyholm, *Quart. Rev. Chem. Soc.* **11**, 339 (1957).
15. B. Darriet and J. Galy, *Acta Crystallogr. Sect.* B **33**, 1489 (1977).
16. G. Bergherhoff, L. Goost, and E. Schultze-Rhonof, *Acta Crystallogr. Sect. B* **24**, 803 (1968).
17. R. R. McDonald, A. C. Larson, and D. T. Cromer, *Acta Crystallogr.* **17**, 1104 (1964).
18. G. Bergheroff and L. Goost, *Acta Crystallogr. Sect. B* **26**, 19 (1970).
19. I. D. Brown, *J. Solid State Chem.* **11**, 214 (1974).
20. R. J. Gillespie, "Molecular geometry," Van Nostrand Reinhold, London (1972).
21. L. E. Orgel, *J. Chem. Soc.*, 3815 (1959).
22. F. Hulliger *in* "Structural Chemistry of Layer-type Phases" (F. Levy Ed.,) Reidel, Dordrecht (1976).

23. A. BYSTRÖM AND K. A. WILHELMI, *Ark. Kemi* **2**, 397 (1950).
24. C. GENEYS, S. VILMINOT, AND L. COT, *Acta Crystallogr. Sect. B* **32**, 3199 (1976).
25. G. DENES, J. PANNETIER, AND J. LUCAS, *C. R. Acad. Sci.* **280**, 835 (1975).
26. A. F. WRIGHT AND A. J. LEADBETTER, *Phil. Mag.* **31**, 1391 (1975).
27. D. R. PEACOR, *Z. Kristallogr. A* **96**, 274 (1973).
28. A. F. WELLS, "Structural Inorganic Chemistry," Clarendon Press, Oxford (1975).
29. W. H. BAUR, *Acta Crystallogr.* **9**, 1515 (1956).
30. S. M. STISHOV AND N. V. BELOV, *Dokl. Akad. Nauk SSR* **143**, 951 (1962).
31. A. PRESINGER, *Naturwissenschaften* **49**, 345 (1962).
32. A. W. BAUR AND A. A. KHAN, *Acta Crystallogr. Sect.* B **27**, 2133 (1971).
33. R. FISCHER AND J. ZEMANN, *Tchermaks Min. Petrol. Mitt.* **22**, 1 (1975).
34. M. O'KEEKE AND B. G. HYDE, *Acta Crystallogr. Sect.* B **22**, 2923 (1976).
35. N. BARTLETT AND K. C. YU, *Canad. J. Chem.* **39**, 80 (1961).